Research Article | Vol. 32, No. 5 / 26 Feb 2024 / Optics Express 8484

Optics EXPRESS

Pure optical twist with zero net torque

ZHENYU HAN,[1] LEI ZHANG,[2,3] XIAO LI,[4] YAXIN LI,[1] TIANTAO QU,[1] XINNING YU,[5] XUDONG YU,[6] JACK NG,[4,9] ZHIFANG LIN,[7,8] AND JUN CHEN[1,3,10]

[1]*State Key Laboratory of Quantum Optics and Quantum Optics Devices, Institute of Theoretical Physics, Shanxi University, Taiyuan, China*
[2]*State Key Laboratory of Quantum Optics and Quantum Optics Devices, Institute of Laser Spectroscopy, Shanxi University, Taiyuan, China*
[3]*Collaborative Innovation Center of Extreme Optics, Shanxi University, Taiyuan, China*
[4]*Department of Physics, Southern University of Science and Technology, Shenzhen, Guangdong, China*
[5]*School of Science, Zhejiang University of Science and Technology, Hangzhou, China*
[6]*State Key Laboratory of Quantum Optics and Quantum Optics Devices, Institute of Opto-Electronics, Shanxi University, Taiyuan, China*
[7]*State Key Laboratory of Surface Physics, Key Laboratory of Micro and Nano Photonic Structures and Department of Physics, Fudan University, Shanghai, China*
[8]*Collaborative Innovation Center of Advanced Microstructures, Nanjing University, Nanjing, China*
[9]*wuzh3@sustech.edu.cn*
[10]*chenjun@sxu.edu.cn*

Abstract: In photonic systems, bilayer or multilayer systems exhibit numerous exciting phenomena induced by twisting. Thus, it is highly desired to explore the twisting effect by engineering the light-matter interactions. Optical torque, an important means in optical micromanipulation, can rotate micro-objects in various ways, enabling a wide range of promising applications. In this study, we present an interesting phenomenon called "pure optical twist" (POT), which emerges when a bilayer structure with specific symmetry is illuminated by counter-propagating lights with opposite spin and/or orbital angular momentum. Remarkably, this leads to zero net optical torque but yet possesses an interesting mechanical effect of bilayer system twisting. The crucial determinant of this phenomenon is the rotational symmetries of each layer, which govern the allowed azimuthal channels of the scattered wave. When the rotational symmetries do not allow these channels to overlap, no resultant torque is observed. Our work will encourage further exploration of the twisting effect through engineered light-matter interactions. This opens up the possibility of creating twisted bilayer systems using optical means, and constructing a stable bilayer optical motor that maintains identical rotation frequencies for both layers.

1. Introduction

Objects, in general, experience optical torque when exposed to an external optical field, as has been extensively studied [1–3]. As an important means in optical micromanipulation [4–11], optical torque [12,13] can rotate micro-objects in different ways [14–16]. It is capable of doing mechanical work and can provide various promising applications, such as optical spanners [17,18], optical motors [19–22], optical matter machines [2,23–25], among others [26–29]. However, zero optical torque typically requires a force that acts through the center of mass, or the particle possessing pertinent symmetries, or just happens by chance, such as when the torque is switching signs. Here we identified a new mechanism that enforces zero net optical torque but yet produces an interesting mechanical effect of bilayer system twisting. This could assist in constructing a stable bilayer optical motor that keeps the rotation frequencies identical for both layers. Moreover, in photonic systems, bilayer or multilayer material systems exhibit numerous exciting phenomena induced by twisting [30,31], such as broadband strongly bianisotropic responses [32], photonic

#518075 https://doi.org/10.1364/OE.518075
Journal © 2024 Received 10 Jan 2024; revised 5 Feb 2024; accepted 11 Feb 2024; published 23 Feb 2024

Optics EXPRESS

topological transition [33–35], and so on [36,37]. Thus, it is highly desired to explore the twisting effect by engineering the light-matter interactions [38,39].

In this work, we consider an arbitrary bilayer structure, where the upper and lower layers are identical and have the degree of rotational symmetry m_s. The bilayer structure laying on the xy-plane is illuminated by two incident lights propagating along $\pm z$ direction with opposite spin and/or orbital angular momentum [see Fig. 1(a) as an example]. In certain bilayer structures with specific m_s, the optical torque acting on each layer can be equal and opposite during rotation, irrespective of their relative orientation or the overall symmetry of the system. This optical twist with zero net optical torque is referred as pure optical twist (POT), which is an analogy definition with the pure spin current (a flow of spins without any net charge current) in condensed matter physics. The POT relies on the rotational symmetry of each layer rather than other structural details. Whereas certain rotational symmetries of bilayer systems presenting robust POT are closely related to the azimuthal channels of each incident light, which is determined by the angular analogue of Floquet's theorem [40–42]. We will first numerically demonstrate the existence of POT by full-wave simulations and then analytically formulate its underlying principle.

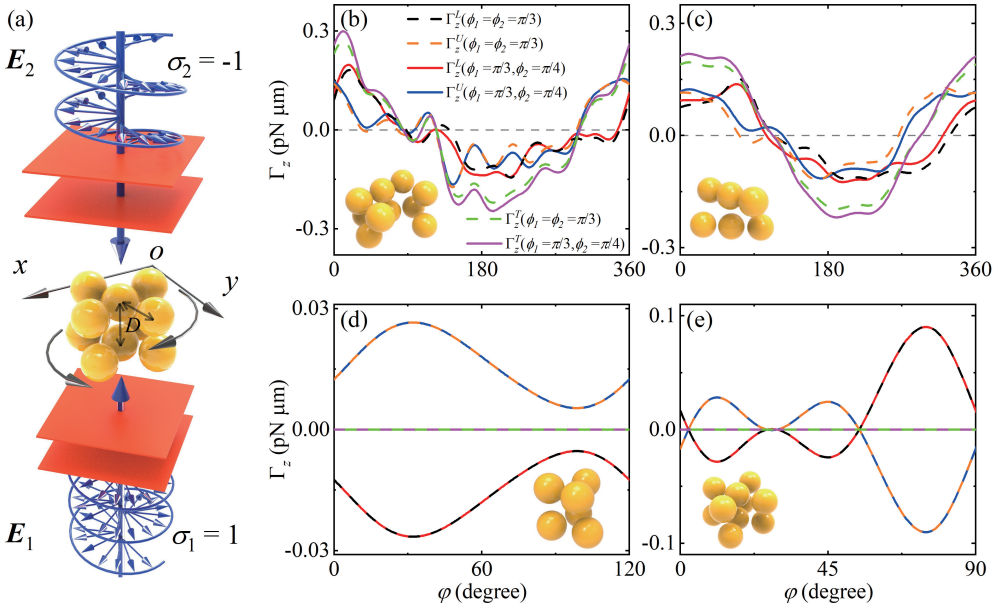

Fig. 1. (a) Schematic of a bilayer structure illuminated by two counter-propagating circularly polarized plane waves with opposite helicities. (b)-(e) Optical torques versus the twist angle φ for bilayer structures with different degrees of rotational symmetry $m_s = 1, 2, 3$, and 4. The structures are depicted in the insets. The permittivity of dielectric spheres is $\varepsilon = 12.25$ [43,44] with the radius $R = 100$ nm. The nearest sphere distance within the same layer and the interlayer distance are arbitrarily set to $D = 2R + 300$ nm (center of sphere to center of sphere). The wavelength and intensity of each incident light are $\lambda = 532$ nm and 1 mW/μm^2, respectively.

2. Pure optical twist in bilayer systems

To enhance clarity and comprehension, we begin by considering an incident light composed of two counter-propagating plane waves with opposite helicities ($\sigma_1 = 1$, $\sigma_2 = -1$) [41,45], as

Optics EXPRESS

illustrated in Fig. 1(a). The electric fields of the two plane waves are expressed as

$$\begin{aligned} \boldsymbol{E}_1 &= \frac{1}{\sqrt{2}} E_0 \left(\boldsymbol{e}_x + i\boldsymbol{e}_y\right) e^{i(kz+\phi_1)}, \\ \boldsymbol{E}_2 &= \frac{1}{\sqrt{2}} E_0 \left(\boldsymbol{e}_x - i\boldsymbol{e}_y\right) e^{-i(kz+\phi_2)}, \end{aligned} \tag{1}$$

where ϕ_1 and ϕ_2 are constant phases, and the time dependence $e^{-i\omega t}$ has been assumed and omitted for simplicity. Later, we will also analyze more scenarios involving counter-propagating waves carrying spin and/or orbital angular momentum.

For the ease and accuracy of computation and interpretation, we start by considering a bilayer structure consisting of a collection of identical dielectric or metallic spheres. Here, the particle structures are chosen to satisfy different rotational symmetries, disregarding the formation of these structures. The distance between particles is chosen arbitrarily as it doesn't affect the occurrence of the observed phenomena (see Fig. S1 in the Supplement 1). We stress that our conclusion remains valid for a bilayer structure comprising continuous pieces of material, as evidenced later. The two identical and parallel layers of spheres stack along the z direction, with the lower and upper layers laying symmetrically at $z<0$ and $z>0$, respectively. The time-averaged optical torques exerted individually on the upper and lower layers of the bilayer structure are calculated by [44]

$$\boldsymbol{\Gamma}^{U,L} = \sum_{i\in U,L} \left(\boldsymbol{\tau}_i + \boldsymbol{r}_i \times \boldsymbol{F}_i\right), \tag{2}$$

where U/L represents the particle cluster in the upper/lower layer. The torque's origin for each layer is fixed at its center of mass and $\boldsymbol{r}_i$ is the position vector of the i-th sphere measured from the center of mass of each layer.

$$\boldsymbol{F}_i = \iint_{\varsigma_i} \boldsymbol{T} \cdot \boldsymbol{n} dS \tag{3}$$

is the time-averaged optical force exerted on the i-th sphere, ς_i is the surface of the i-th sphere, and $\boldsymbol{n}$ denotes the unit outward normal at surface ς_i.

$$\boldsymbol{\tau}_i = \iint_{\varsigma_i} \left(\boldsymbol{r}_i^{'} \times \boldsymbol{T}\right) \cdot \boldsymbol{n} dS \tag{4}$$

is the torque acting on the i-th sphere about its center, which vanishes when the sphere is non-absorptive. $\boldsymbol{r}_i^{'}$ is the vector from the center of the sphere to the integral surface, and the time-averaged Maxwell stress tensor $\boldsymbol{T}$ can be evaluated by using the generalized Lorentz-Mie scattering theory for multi-spheres [46,47]. In the following, we only focus on the z component of the torque, i.e., $\Gamma_z^{U,L}$ and $\Gamma_z^T = \Gamma_z^U + \Gamma_z^L$, to characterize the twist of the bilayer system.

Figures 1(b)–1(e) show the optical torques $\Gamma_z^{U,L,T}$ versus the twist angle φ between the two layers of bilayer systems with four different rotational symmetries. It is immediately seen that the net optical torques Γ_z^T are in general nonzero, i.e., $\Gamma_z^U \neq -\Gamma_z^L$, for the systems with rotational symmetry $m_s = 1, 2$. In contrast, zero net optical torque is generated for systems with $m_s = 3, 4$, demonstrating POT. Usually, the optical torque can be affected by the phase because altering the phases ϕ_1 and ϕ_2 in Eq. (1) leads to a change in the polarization angle of the optical field and hence the optical torque. Figures 1(b)–1(c) ($m_s = 1, 2$) indeed demonstrate a clear dependence of the optical torque on the phase. However, we observe a strikingly different behavior in Figs. 1(d)–1(e) ($m_s = 3, 4$), where the POT appears to be completely unaffected by any changes in the phase. The phase shift-insensitive POT greatly facilitates the experimental implementation. Moreover, POT demonstrates robustness against weak symmetry breaking caused by the structure. For instance, for the bilayer structure used in Fig. 1(d), POT remains robust even if the two layers

Optics EXPRESS

lack strict three-fold symmetry or exhibit slight differences (see Fig. S2 in the Supplement 1 for more details). This robustness is helpful to experimental observation of the POT phenomenon where imperfect settings always exist.

One can image that, in cases where there is no net angular momentum inflow from the total incident light, the scattered light in a system with certain symmetry can also possess zero net angular momentum, resulting in the system acquiring zero torque. However, the scattering process is complex. In order to rigorously demonstrate the reason behind the absence of net torque (i.e. POT), we resort to the equivalent expression of the optical torque by the T-matrix method [40–42,48],

$$\Gamma_z^T = c_0 \mathrm{Re} \sum_{l=1}^{\infty} \sum_{m=-l}^{l} m \left[p_{ml} a_{ml}^* + q_{ml} b_{ml}^* - \left(|a_{ml}|^2 + |b_{ml}|^2 \right) \right], \tag{5}$$

where $c_0 = 2\pi\varepsilon_0 |E_0|^2 / k^3$. Equation (5) can be derived by extending the integrating sphere in Eq. (4) to encompass the entire bilayer structure, with the center of the integrating sphere set as the center of the entire structure. Additionally, the total electromagnetic fields in the time-averaged Maxwell stress tensor are expanded using vector spherical wave functions [41,49]. p_{ml} and q_{ml} (a_{ml} and b_{ml}) denote the partial wave expansion coefficients [50,51] for incident (scattered) waves (see Supplement 1 for more details). Our calculations are accurate within classical electrodynamics, and the numerical convergence is governed by the maximum angular momentum (set to 60 for the considered size parameters) at which the series expansion was truncated. It is worth noting that p_{ml} and q_{ml} can only be nonzero when m equals its corresponding incident azimuthal channel. This approach allows us to analyze the necessary conditions to generate POT appropriately. Since the incident light is composed of two waves, the partial wave expansion coefficients in Eq. (5) can be rewritten as

$$\chi_{ml} = \chi_{1,ml} + \chi_{2,ml}, \tag{6}$$

where χ denotes p, q, a, and b, and the subscripts 1 and 2 correspond to the first and second incident waves and their respective scattered waves. Then the net optical torque can be divided into three parts by substituting Eq. (6) into Eq. (5)

$$\Gamma_z^T = \Gamma_{1,z} + \Gamma_{2,z} + \Gamma_{3,z}, \tag{7}$$

where

$$\Gamma_{1,z} = c_0 \,\mathrm{Re} \sum_{l=1}^{\infty} \sum_{m=-l}^{l} m \left[p_{1,ml} a_{1,ml}^* + q_{1,ml} b_{1,ml}^* - \left(\left|a_{1,ml}\right|^2 + \left|b_{1,ml}\right|^2 \right) \right], \tag{8a}$$

$$\Gamma_{2,z} = c_0 \,\mathrm{Re} \sum_{l=1}^{\infty} \sum_{m=-l}^{l} m \left[p_{2,ml} a_{2,ml}^* + q_{2,ml} b_{2,ml}^* - \left(\left|a_{2,ml}\right|^2 + \left|b_{2,ml}\right|^2 \right) \right], \tag{8b}$$

$$\begin{aligned} \Gamma_{3,z} = c_0 \,\mathrm{Re} \sum_{l=1}^{\infty} \sum_{m=-l}^{l} m \Big[& p_{1,ml} a_{2,ml}^* + p_{2,ml} a_{1,ml}^* + q_{1,ml} b_{2,ml}^* + q_{2,ml} b_{1,ml}^* \\ & - \left(a_{1,ml} a_{2,ml}^* + a_{2,ml} a_{1,ml}^* + b_{1,ml} b_{2,ml}^* + b_{2,ml} b_{1,ml}^* \right) \Big]. \end{aligned} \tag{8c}$$

The terms $\Gamma_{1,z}$ and $\Gamma_{2,z}$ represent the optical torques generated by the first and second plane waves, respectively. Since the helicities of these two plane waves are opposite, $\Gamma_{1,z}$ and $\Gamma_{2,z}$ cancel each other. Consequently, the net optical torque is solely determined by $\Gamma_{3,z}$, termed the interference contribution. The expression for $\Gamma_{3,z}$ indicates that only partial waves involving the same azimuthal channel m contribute to the z component of the net optical torque.

Optics EXPRESS

According to the angular analogue of the Floquet's theorem [40,41] (see also, Ref. [42] for a simple proof), the allowed azimuthal channels m of the scattered photons from a scatter with the degree of rotational symmetry m_s are

$$m = m_i + n \times m_s, \tag{9}$$

where m_i is the azimuthal channel of the i-th incident wave, with $i = 1, 2$ and $n = 0, \pm1, \pm2, \ldots$. An important consequence of Eq. (9) is that the interference term $\Gamma_{3,z}$ in Eq. (8) does not vanish only when the degree of the system's rotational symmetry m_s satisfies

$$m_s = \left|\frac{m_1 - m_2}{N}\right|, \tag{10}$$

where N is an integer. When using the incident fields described by Eq. (1) with the incident azimuthal channel $m_1 = 1$ and $m_2 = -1$ [24,42,49], Fig. 2 illustrates the allowed azimuthal channels of scattered photons when the incident light is scattered by a bilayer structure with m_s degrees of rotational symmetry. The first row of circles represents the azimuthal channels when the incident light with azimuthal channel $m_1 = 1$ is scattered by the bilayer structure. Similarly, the second row of circles represents the azimuthal channels when the counter-propagating incident light with azimuthal channel $m_2 = -1$ is scattered by the same structure. For bilayer structures with a degree of rotational symmetry of $m_s = 1$ or 2, circles with the same value can be found from the upper and lower rows. For example, when $m_s = 1$, the value of circle $1 - 3 \times m_s$ in the first row equals $-1 - 1 \times m_s$ in the second row. These circles are connected by a red line. Similarly, for $m_s = 2$, the value of circle $1 - 3 \times m_s$ in the first row equals $-1 - 2 \times m_s$ in the second row, and they are connected by a blue line. However, for bilayer structures with rotational symmetry of $m_s = 3$ or larger, circles with the same value cannot be found in these two rows. Instead, they are represented by green cross lines. Therefore, only systems with the degree of rotational symmetry $m_s = 1$ and 2 are capable of scattering both incident waves into identical azimuthal channels, thus contributing to the value of $\Gamma_{3,z}$. While for $m_s \geq 3$, the angular analogue of the Floquet's theorem [Eq. (9)] and its resultant condition [Eq. (10)] prohibit the two incident waves from being scattered into the same azimuthal channel m.

Consequently, this leads to the vanishing of the interference torque $\Gamma_{3,z}$ and, in turn, the vanishing of the POT. The vanishing of $\Gamma_{3,z}$ for $m_s \geq 3$ can be understood as the scattered fields from both layers are "orthogonal" in terms of angular momentum calculation. As a result, POT is immune to the phase shift in both beams, as illustrated in Figs. 1(d) and 1(e). As its underlying physics originates fundamentally from the rotational symmetry of the structure, the POT is not limited to a system composed of spherical particles, as will be shown latter. Moreover, Eqs. (7)–(8) can be applied to structures consisting of any number of layers. As long as the rotational symmetry of the structure does not satisfy Eq. (10), the total optical torque can be ensured to be zero, that is, the occurrence of POT (see Fig. S3 in the Supplement 1 for more details).

Before moving on to more generalized cases, we discuss the possibility of the POT for the structure with m_s<3, which is subjected to counter-propagating plane waves illumination. Are there any special cases for structures with m_s<3 that can generate POT? In other words, how can POT be achieved for a bilayer structure whose symmetry satisfies Eq. (10)? In Figs. 3(a) and 3(b), we present optical torques as functions of the phase difference ($\Delta\phi = \phi_2 - \phi_1$, ϕ_1 is, for example, fixed to $\pi/3$) for systems with the degree of rotational symmetry $m_s = 3$ and $m_s = 2$, respectively, while arbitrarily choosing the twist angle φ as 130°. Figure 3(a) confirms that for $m_s = 3$, $\Gamma_z^L = -\Gamma_z^U$ holds true regardless of the phase difference $\Delta\phi$. However, for the system with $m_s = 2$, Fig. 3(b) shows that Γ_z^L and $-\Gamma_z^U$ are generally different due to the presence of the non-zero interference term $\Gamma_{3,z}$. Interestingly, at specific points such as $\Delta\phi = \pi/3, 4\pi/3$, the net optical torque can also be zero with $\Gamma_z^L = -\Gamma_z^U$. Further analysis of individual partial wave

Optics EXPRESS

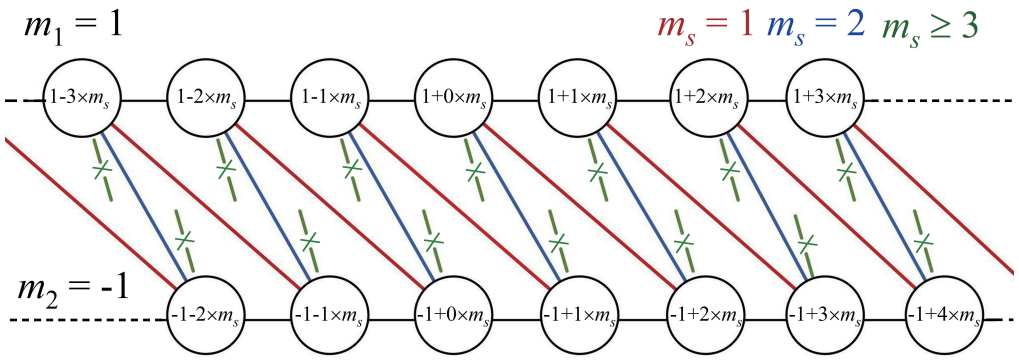

Fig. 2. The circles represent the allowed azimuthal channels of scattered photons when incident lights, described by Eq. (1), are scattered by a bilayer structure. The upper/lower row of circles corresponds to the azimuthal channels when incident light with azimuthal channel $m_1 = 1/m_2 = -1$ is scattered by a bilayer structure with a rotational symmetry of m_s. For bilayer structures with rotational symmetry of $m_s = 1$ or 2, circles with the same value can be found in both rows, connected by red or blue lines, indicating that they correspond to the same azimuthal channel. However, for bilayer structures with rotational symmetry of $m_s = 3$ or larger, circles with the same value cannot be found in these two rows, represented by green cross lines, indicating that the same azimuthal channel of scattered photons cannot be generated.

azimuthal channels in $\Gamma_{3,z}$ reveals that contributions from channels $\pm m$ cancel each other at these particular phase differences. Figure 3(c) illustrates the contributions from dominant azimuthal channels in $\Gamma_{3,z}$ when $\Delta\phi = \pi/3$, corresponding to the red star in Fig. 3(b). The contributions from $m = 1, 3$ precisely opposite those from $m = -1, -3$, resulting in a zero net optical torque. It is worth noting that both the total incident field of Eq. (1) situated on the bilayer structure planes [$z = \pm D/2$, represented by the red arrows in the inset of Fig. 3(c)] and the bilayer structure itself [represented by the black lines in the inset of Fig. 3(c)] exhibit mirror symmetry with respect to the y direction when projected on the xy-plane in this situation. Other special points with zero net optical torque correspond to "mirror" symmetries along either the x or y directions. Furthermore, we explicitly present the results for $\Delta\phi = 2\pi/3$ [blue stars in Fig. 3(b)] in Fig. 3(d). Here, the contributions from m and $-m$ no longer cancel each other since the total incident field lose "mirror" symmetry along the x and y directions, as shown in the inset of Fig. 3(d). This finding reveals the crucial role of "mirror" symmetry [40] in achieving the POT when the resultant condition of the angular Floquet's theorem [Eq. (10)] is satisfied. It represents a typical scenario where the POT occurs "accidentally". In the following, we will exclude this "accidental" case induced by the particular phase difference and focus on the POT that is due to the symmetry and immune to the phase.

Next, we investigate POT on a bilayer structure in the illumination of beams carrying both orbital angular momentum (OAM) and spin angular momentum (SAM). The Laguerre-Gaussian (LG) beams [40,41] serve best for this purpose. When two linearly polarized counter-propagating LG beams carry OAM characterized by $l_1 = 3$, $l_2 = -3$ [40], the corresponding incident azimuthal channels are $m_1 = l_1 \pm 1 = 2, 4$ and $m_2 = l_2 \pm 1 = -2, -4$. Here, the ± 1 values correspond to linear polarization (see Sec. 2 in the Supplement 1), which can be considered as a superposition of circular polarizations with $\sigma = 1$ and -1. Thus $m_1 - m_2$ take values of $4, 6, 8$. According to Eq. (10), there will not be POT if m_s is a divisor of $m_1 - m_2$. Therefore, POT will occur for $m_s = 5, 7, 9$, and so on, as illustrated in Fig. 4(a) (depicted as blue dots), obtained through numerical calculations based on the multi-spheres scattering theory [46,47]. On the other hand, when the two LG beams are circularly polarized with $\sigma_1 = 1$ and $\sigma_2 = -1$, the incident azimuthal

Optics EXPRESS

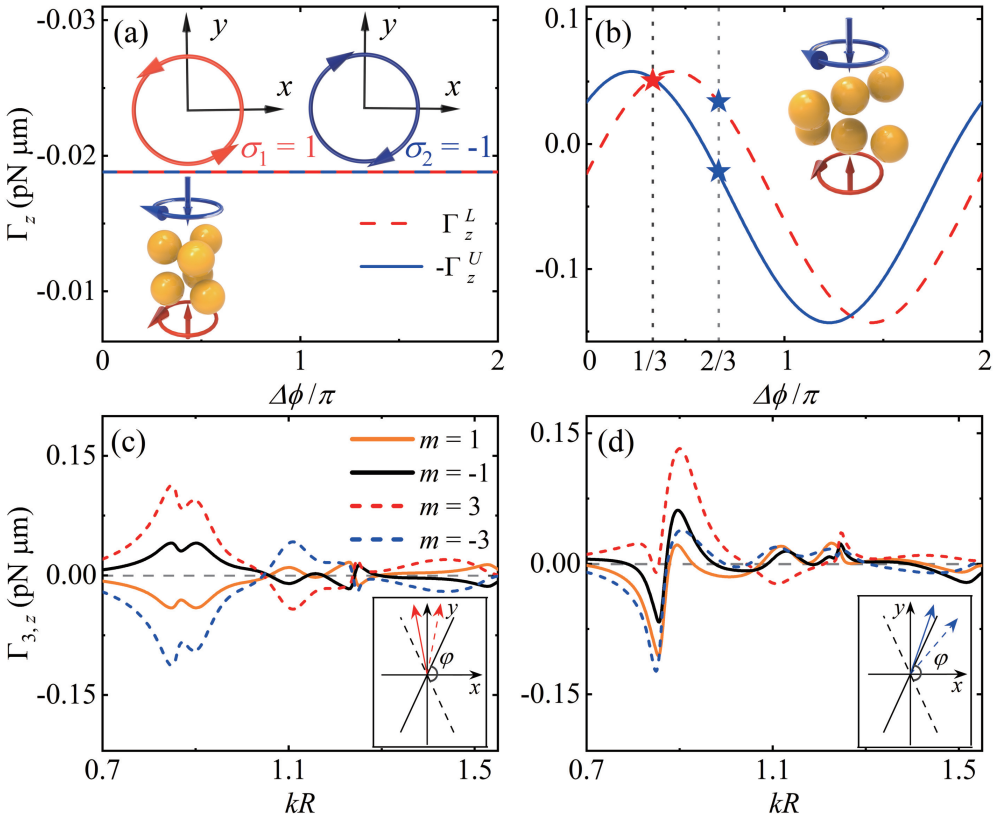

Fig. 3. Optical torques exerted on the lower and upper (opposite value of Γ_z^U is taken to facilitate comparison) layers of a bilayer system (twist angle $\varphi = 130°$) versus the phase difference $\Delta\phi$ are shown in (a) $m_s = 3$ and (b) $m_s = 2$. The wavelength and intensity of the two incident counter-propagating plane waves ($\sigma_1 = 1$, $\sigma_2 = -1$) is $\lambda = 532$ nm and 1 mW/μm^2, respectively. For $m_s = 2$, the contributions to the torque $\Gamma_{3,z}$ by individual dominant partial wave azimuthal channels are depicted versus kR in panels (c) and (d) for $\Delta\phi = \pi/3$ and $\Delta\phi = 2\pi/3$, respectively. In the insets of (c) and (d), the black solid lines and dashed lines represent the upper and lower layers of the bilayer structure with $m_s = 2$ projected onto the xy-plane, respectively. These lines can be visualized as the axis passing through the three spheres in each layer. The red/blue solid line arrow or dashed arrow in the insets of (c)/(d) indicates the direction of the total incident field projected onto the xy-plane at $z = D/2$ or $z = -D/2$. Other parameters of the system are $\varepsilon = 12.25$, $R = 100$ nm, and $D = 500$ nm.

channels are $m_1 = l_1 + \sigma_1 = 4$ and $m_2 = l_2 + \sigma_2 = -4$. Following Eq. (10), the POT will show up when m_s is not a divisor of $m_1 - m_2 = 8$. In other words, the POT occurs for $m_s = 3, 5, 6, 7, 9$, and so forth, as corroborated by numerical results (denoted by red squares) in Fig. 4(a). Furthermore, in the case where $l_1 = 1$, $l_2 = -1$, $\sigma_1 = -1$, and $\sigma_2 = 1$, we find that $m_1 = m_2 = 0$, resulting in any m_s being a divisor of $m_1 - m_2 = 0$. Consequently, the production of the POT becomes impossible for any structures under these conditions, as illustrated in Fig. 4(b). Table 1 showcases additional instances of counter-propagating waves carrying spin and/or orbital angular momentum.

Our analysis reveals that the emergence of the POT is solely dependent on the appropriate symmetry of the system, irrespective of other system details. To further validate this finding, we examine a bilayer structure comprising two absorptive gold square plates (instead of sphere

Optics EXPRESS

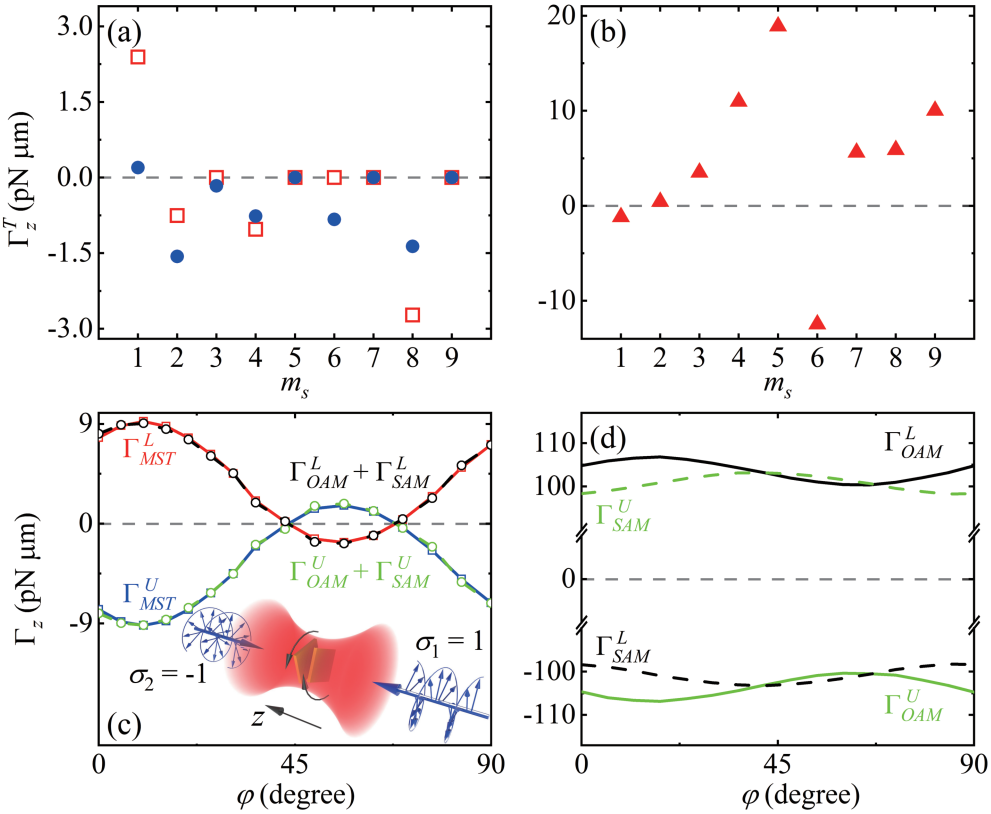

Fig. 4. The net optical torque exerted on a bilayer structure composed of identical silver [44] spheres (R = 100 nm, $D = 2R$+200 nm, twist angle $\varphi = 30°$) illuminated by counter-propagating LG beams (numerical aperture NA = 0.6, beam power 0.1 W, λ =532 nm, and phase shift $\phi_1 = \pi/3$, $\phi_2 = \pi/4$) versus m_s are shown in (a) $l_1 = 3$, $l_2 = -3$ and (b) $l_1 = 1$, $l_2 = -1$, $\sigma_1 = -1$, $\sigma_2 = 1$. The structures of $m_s = 1, 2, 3, 4$ use the same structures as those shown in Figs. 1(b)-1(e), and structures of $m_s = 5, 6, 7, 8, 9$ are rings composed of m_s spheres, see also Fig. S4 in the Supplement 1. The blue dots and red squares in (a) correspond to LG beams with x-polarized linear ($\sigma_1 = \sigma_2 = 0$) and circular ($\sigma_1 = 1$, $\sigma_2 = -1$) polarizations, respectively. (c) Optical torques calculated via two different approaches exerted on the upper and lower plates of a bilayer structure with $m_s = 4$ versus the twist angle φ. The schematic plot of the whole optical system is shown in the inset. The bilayer structure consists of two identical 30 nm thick square-shaped gold [20] plates separated by a gap of 86 nm, with an area of 255 × 255 nm^2. The incident light constitutes of two counter-propagating circularly polarized Gaussian beams with opposite helicities (NA = 0.6, λ = 1064 nm, beam power 0.1 W, and phase shift $\phi_1 = \pi/3$, $\phi_2 = \pi/4$). (d) Optical torques exerted on the upper and lower plates of the bilayer structure contributed by the SAM and OAM.

aggregate), illuminated by two circularly polarized counter-propagating Gaussian beams with opposite helicities [see the inset of Fig. 4(c)]. In this case, one has $m_1 = 1$ and $m_2 = -1$, Eq. (10) indicates the presence of POT for the $m_s = 4$ system. Figure 4(c) indeed exhibits the POT phenomenon, confirming that POT is only determined by the symmetry governed by the angular analogue of Floquet's theorem and is not influenced by other system particulars. Here, the total electromagnetic fields are obtained by using a commercial finite-element-method package COMSOL Multiphysics (http://www.comsol.com/). The torques are obtained through direct

Optics EXPRESS

Table 1. The degree of rotational symmetry m_s for systems producing robust POT in linearly polarized (LP) or circularly polarized (CP) counter-propagating Gaussian or Laguerre-Gaussian (LG) beams. Here, N is an integer.

Polarization / Incident beams	LP ($\sigma_1 = \sigma_2 = 0$)	CP ($\sigma_1 = 1$, $\sigma_2 = -1$)	CP ($\sigma_1 = -1$, $\sigma_2 = 1$)
Gaussian beams ($l_1 = l_2 = 0$)	None	m_s = 3, 4, 5, 6, 7, 8, 9, ...	m_s = 3, 4, 5, 6, 7, 8, 9, ...
LG beams ($l_1 = 1$, $l_2 = -1$)	None	m_s = 3, 5, 6, 7, 8, 9, ...	None
LG beams ($l_1 = 2$, $l_2 = -2$)	m_s = 5, 7, 8, 9, ...	m_s = 4, 5, 7, 8, 9, ...	m_s = 3, 4, 5, 6, 7, 8, 9, ...
LG beams ($l_1 = 3$, $l_2 = -3$)	m_s = 5, 7, 9, ...	m_s = 3, 5, 6, 7, 9, ...	m_s = 3, 5, 6, 7, 8, 9, ...
LG beams ($l_1 = l$, $l_2 = -l$)	$m_s \neq \lvert 2l / N \rvert$, $\lvert (2l+2) / N \rvert$, $\lvert (2l-2) / N \rvert$	$m_s \neq \lvert (2l+2) / N \rvert$	$m_s \neq \lvert (2l-2) / N \rvert$

calculations from Maxwell's theory (Γ_{MST}) [42,52], as well as by integrating the SAM and OAM current densities (denoted as Γ_{SAM} and Γ_{OAM}, respectively, see Sec. 4 in Supplement 1 for the expressions of SAM and OAM current densities [53]). The results obtained through these two methods agree well. In addition, by comparing Fig. 1(e) and Fig. 4(c), it can be seen that for structures with rotational symmetry $m_s = 4$, the number of peaks for the optical torque exerted on each layer differs within one period (the twist angle φ runs from 0° to 90°). Strong interlayer coupling enhances the torque exerted on each layer. The enhanced coupling is related to both the symmetry and the specific details of the structure. Specifically, the number of maximum values for optical torque on each layer are determined by the structure's symmetry, while the number of minor peaks is also associated with the structure's details (see Fig. S5 and Fig. S6 in the Supplement 1 for more details).

Finally, we explore the conversion between SAM and OAM when the POT occurs. The conversion of SAM to OAM can occur when light is scattered by particles [54,55]. Figures 4(c) and 4(d) use nearly paraxial (numerical aperture NA = 0.6) circularly polarized Gaussian beams. In this context, the incident lights can be regarded as carrying only SAM (refer to Fig. S7 in Supplement 1). However, as depicted in Fig. 4(d), both SAM and OAM contribute to the optical torque in each layer. This indicates that, for each layer, a conversion from spin angular momentum to orbital angular momentum occurs, and the resulting difference contributes to the torque experienced by that layer. Specifically, the conversion between SAM and OAM occurs at individual layer but not on the entire system. As depicted in Figs. 4(c) and 4(d), the lower plate acquires negative SAM from the field while radiating OAM (acquiring positive OAM), manifesting itself as a partial conversion from SAM to OAM, with the difference contributing to Γ_z^L. Interestingly, the upper plate does the opposite and completely compensates for the consequence caused by the lower plate, thus resulting in the individual conservation of SAM and OAM of the illuminating field while leaving us with a POT in the system.

Optics EXPRESS

3. Conclusion

In conclusion, we identified a new mechanism that enforces zero net optical torque but yet possesses an interesting mechanical effect of bilayer system twisting. This intriguing behavior, which we refer to as POT, manifests as the optical torque exerted on each layer of a bilayer structure being exactly equal in magnitude but opposite in direction during rotation. The underlying mechanism can be traced to the angular analogue of Floquet's theorem, which dictates the possible azimuthal channels of the scattered waves from both layers. When these scattered waves from both layers are "orthogonal", meaning they possess different azimuthal numbers and cannot interfere, the POT is generated. As the POT stems from the system's inherent symmetry rather than its specific details, it is believed to be universal and fundamentally different from the accidental vanishing of the optical torque. Our work enhances the understanding of light-matter interactions and opens up the new possibility for developing twisted bilayer structure systems with optical means, a stable bilayer optical motor for DNA unfolding, etc.

Funding. National Natural Science Foundation of China (12174231, 12074084, 12074169, 12074230); Fundamental Research Program of Shanxi Province (202103021222001); Fund for Shanxi 1331 Project; Research Project Supported by Shanxi Scholarship Council of China; Stable Support Plan Program of Natural Science Foundation of Shenzhen Municipality (20200925152152003); Program of Education and Teaching Reform in Shanxi Province (J20230003).

Disclosures. The authors declare no conflicts of interest.

Data availability. Data underlying the results presented in this paper are not publicly available at this time but may be obtained from the authors upon reasonable request.

Supplemental document. See Supplement 1 for supporting content.

References

1. S. Kuhn, B. A. Stickler, A. Kosloff, *et al.*, "Optically driven ultra-stable nanomechanical rotor," Nat. Commun. **8**(1), 1670 (2017).
2. F. Han, J. A. Parker, Y. Yifat, *et al.*, "Crossover from positive to negative optical torque in mesoscale optical matter," Nat. Commun. **9**(1), 4897 (2018).
3. Q. Sun, K. Dholakia, and A. D. Greentree, "Optical forces and torques on eccentric nanoscale core–shell particles," ACS Photonics **8**(4), 1103–1111 (2021).
4. A. Ashkin, J. M. Dziedzic, J. E. Bjorkholm, *et al.*, "Observation of a single-beam gradient force optical trap for dielectric particles," Opt. Lett. **11**(5), 288–290 (1986).
5. K. Dholakia and P. Reece, "Optical micromanipulation takes hold," Nano Today **1**(1), 18–27 (2006).
6. J. Chen, J. Ng, Z. F. Lin, *et al.*, "Optical pulling force," Nat. Photonics **5**(9), 531–534 (2011).
7. J. Millen, T. Deesuwan, P. Barker, *et al.*, "Nanoscale temperature measurements using non-equilibrium brownian dynamics of a levitated nanosphere," Nat. Nanotechnol. **9**(6), 425–429 (2014).
8. P. Shi, L. P. Du, and X. C. Yuan, "Structured spin angular momentum in highly focused cylindrical vector vortex beams for optical manipulation," Opt. Express **26**(18), 23449–23459 (2018).
9. W. Q. Ding, T. T. Zhu, L. M. Zhou, *et al.*, "Photonic tractor beams: A review," Adv. Photonics **1**(02), 1 (2019).
10. H. Li, Y. Y. Cao, L. M. Zhou, *et al.*, "Optical pulling forces and their applications," Adv. Opt. Photonics **12**(2), 288–366 (2020).
11. M. Peng, H. Luo, W. Xiong, *et al.*, "Enhanced optical trapping of ZrO_2@TiO_2 photonic force probe with broadened solvent compatibility," Opt. Express **30**(26), 46060–46069 (2022).
12. T. L. Qi, F. Han, W. B. Liu, *et al.*, "Stable negative optical torque in optically bound nanoparticle dimers," Nano Lett. **22**(21), 8482–8486 (2022).
13. F. Nan, X. Li, S. L. Zhang, *et al.*, "Creating stable trapping force and switchable optical torque with tunable phase of light," Sci. Adv. **8**(46), eadd6664 (2022).
14. J. P. Zheng, S. H. Lam, H. Huang, *et al.*, "Recent progress in optical-resonance-assisted movement control of nanomotors," Adv. Intell. Syst. **2**(3), 1900160 (2020).
15. W. Lyu, W. W. Tang, W. Yan, *et al.*, "Light-induced in-plane rotation of microobjects on microfibers," Laser Photonics Rev. **16**(5), 2100561 (2022).
16. W. Q. Li, X. Wang, J. M. Liu, *et al.*, "Flexible control of an ultrastable levitated orbital micro-gyroscope through orbital-translational coupling," Nanophotonics **12**(7), 1245–1253 (2023).
17. N. B. Simpson, L. Allen, and M. J. Padgett, "Optical tweezers and optical spanners with Laguerre-Gaussian modes," J. Mod. Opt. **43**(12), 2485–2491 (1996).
18. A. T. O'Neil and M. J. Padgett, "Three-dimensional optical confinement of micron-sized metal particles and the decoupling of the spin and orbital angular momentum within an optical spanner," Opt. Commun. **185**(1-3), 139–143 (2000).

Optics EXPRESS

19. P. Galajda and P. Ormos, "Complex micromachines produced and driven by light," Appl. Phys. Lett. **78**(2), 249–251 (2001).
20. M. Liu, T. Zentgraf, Y. M. Liu, *et al.*, "Light-driven nanoscale plasmonic motors," Nat. Nanotechnol. **5**(8), 570–573 (2010).
21. T. Wu, T. A. Nieminen, S. Mohanty, *et al.*, "A photon-driven micromotor can direct nerve fibre growth," Nat. Photonics **6**(1), 62–67 (2012).
22. L. L. Xu, F. Z. Mou, H. T. Gong, *et al.*, "Light-driven micro/nanomotors: From fundamentals to applications," Chem. Soc. Rev. **46**(22), 6905–6926 (2017).
23. P. McCormack, F. Han, and Z. J. Yan, "Self-organization of metal nanoparticles in light: Electrodynamics–molecular dynamics simulations and optical binding experiments," J. Phys. Chem. C **9**(3), 545–549 (2018).
24. J. Parker, C. W. Peterson, Y. Yifat, *et al.*, "Optical matter machines: Angular momentum conversion by collective modes in optically bound nanoparticle arrays," Optica **7**(10), 1341–1348 (2020).
25. F. Han and Z. J. Yan, "Phase transition and self-stabilization of light-mediated metal nanoparticle assemblies," ACS Nano **14**(6), 6616–6625 (2020).
26. L. Paterson, M. P. MacDonald, J. Arlt, *et al.*, "Controlled rotation of optically trapped microscopic particles," Science **292**(5518), 912–914 (2001).
27. K. Lin, I. Tutunnikov, J. Ma, *et al.*, "Spatiotemporal rotational dynamics of laser-driven molecules," Adv. Photonics **2**(02), 1 (2020).
28. H. B. Xin, Y. C. Li, Y. C. Liu, *et al.*, "Optical forces: From fundamental to biological applications," Adv. Mater. **32**(37), 2001994 (2020).
29. F. Strasser, S. M. Barnett, M. Ritsch-Marte, *et al.*, "Generally applicable holographic torque measurement for optically trapped particles," Phys. Rev. Lett. **128**(21), 213604 (2022).
30. W. Ma, F. Cheng, and Y. M. Liu, "Deep-learning-enabled on-demand design of chiral metamaterials," ACS Nano **12**(6), 6326–6334 (2018).
31. J. Duan, G. Álvarez-Pérez, C. Lanza, *et al.*, "Multiple and spectrally robust photonic magic angles in reconfigurable α-MoO_3 trilayers," Nat. Mater. **22**(7), 867–872 (2023).
32. Y. Zhao, M. A. Belkin, and A. Alù, "Twisted optical metamaterials for planarized ultrathin broadband circular polarizers," Nat. Commun. **3**(1), 870 (2012).
33. O. V. Kotov and Y. E. Lozovik, "Hyperbolic hybrid waves and optical topological transitions in few-layer anisotropic metasurfaces," Phys. Rev. B **100**(16), 165424 (2019).
34. G. W. Hu, A. Krasnok, Y. Mazor, *et al.*, "Moiré hyperbolic metasurfaces," Nano Lett. **20**(5), 3217–3224 (2020).
35. G. W. Hu, Q. D. Ou, G. Y. Si, *et al.*, "Topological polaritons and photonic magic angles in twisted α-MoO_3 bilayers," Nature **582**(7811), 209–213 (2020).
36. H. X. Xu, G. W. Hu, L. Han, *et al.*, "Chirality-assisted high-efficiency metasurfaces with independent control of phase, amplitude, and polarization," Adv. Opt. Mater. **7**(4), 1801479 (2019).
37. G. W. Hu, M. S. Wang, Y. Mazor, *et al.*, "Tailoring light with layered and moiré metasurfaces," Trends Chem. **3**(5), 342–358 (2021).
38. L. Xu, M. Rahmani, Y. Ma, *et al.*, "Enhanced light–matter interactions in dielectric nanostructures via machine-learning approach," Adv. Photonics **2**(02), 1 (2020).
39. X. H. Xu, Y. Yang, L. X. Chen, *et al.*, "Optomechanical wagon-wheel effects for bidirectional sorting of dielectric nanoparticles," Laser Photonics Rev. **15**(6), 2000546 (2021).
40. T. A. Nieminen, S. J. W. Parkin, N. R. Heckenberg, *et al.*, "Optical torque and symmetry," Proc. SPIE **5514**, 254–263 (2004).
41. T. A. Nieminen, T. Asavei, V. L. Loke, *et al.*, "Symmetry and the generation and measurement of optical torque," J. Quant. Spectrosc. Radiat. Transfer **110**(14-16), 1472–1482 (2009).
42. J. Chen, J. Ng, K. Ding, *et al.*, "Negative optical torque," Sci. Rep. **4**(1), 6386 (2014).
43. J. J. Du, Z. F. Lin, S. T. Chui, *et al.*, "Optical beam steering based on the symmetry of resonant modes of nanoparticles," Phys. Rev. Lett. **106**(20), 203903 (2011).
44. J. Chen, N. Wang, L. Y. Cui, *et al.*, "Optical twist induced by plasmonic resonance," Sci. Rep. **6**(1), 27927 (2016).
45. K. Y. Bliokh, A. Y. Bekshaev, and F. Nori, "Extraordinary momentum and spin in evanescent waves," Nat. Commun. **5**(1), 3300 (2014).
46. Y. L. Xu, "Electromagnetic scattering by an aggregate of spheres," Appl. Opt. **34**(21), 4573–4588 (1995).
47. Y. L. Xu, "Electromagnetic scattering by an aggregate of spheres: Far field," Appl. Opt. **36**(36), 9496–9508 (1997).
48. T. A. Nieminen, V. L. Loke, A. B. Stilgoe, *et al.*, "T-matrix method for modelling optical tweezers," J. Mod. Opt. **58**(5-6), 528–544 (2011).
49. J. Chen, S. Wang, X. Li, *et al.*, "Mechanical effect of photonic spin-orbit interaction for a metallic nanohelix," Opt. Express **26**(21), 27694–27704 (2018).
50. J. Ng, Z. F. Lin, C. T. Chan, *et al.*, "Photonic clusters formed by dielectric microspheres: Numerical simulations," Phys. Rev. B **72**(8), 085130 (2005).
51. T. A. Nieminen, V. L. Y. Loke, A. B. Stilgoe, *et al.*, "Optical tweezers computational toolbox," J. Opt. A: Pure Appl. Opt. **9**(8), S196–S203 (2007).
52. Y. Z. Shi, T. T. Zhu, A. Q. Liu, *et al.*, "Inverse optical torques on dielectric nanoparticles in elliptically polarized light waves," Phys. Rev. Lett. **129**(5), 053902 (2022).

Optics EXPRESS

53. Y. K. Jiang, H. J. Chen, J. Chen, *et al.*, "Universal relationships between optical force/torque and orbital versus spin momentum/angular momentum of light," arXiv, arXiv:1511.08546 (2015).
54. K. Y. Bliokh, F. J. Rodríguez-Fortuño, F. Nori, *et al.*, "Spin–orbit interactions of light," Nat. Photonics **9**(12), 796–808 (2015).
55. B. Wang, W. Liu, M. Zhao, *et al.*, "Generating optical vortex beams by momentum-space polarization vortices centred at bound states in the continuum," Nat. Photonics **14**(10), 623–628 (2020).